IEEE Photonics Journal
An IEEE Photonics Society Publication

Open Access

# Investigation and Improvement of 90° Direct Bends of Metal–Insulator–Silicon–Insulator–Metal Waveguides

Volume 5, Number 5, October 2013

**Jin-Soo Shin**
**Min-Suk Kwon**
**Chang-Hee Lee**
**Sang-Yung Shin**

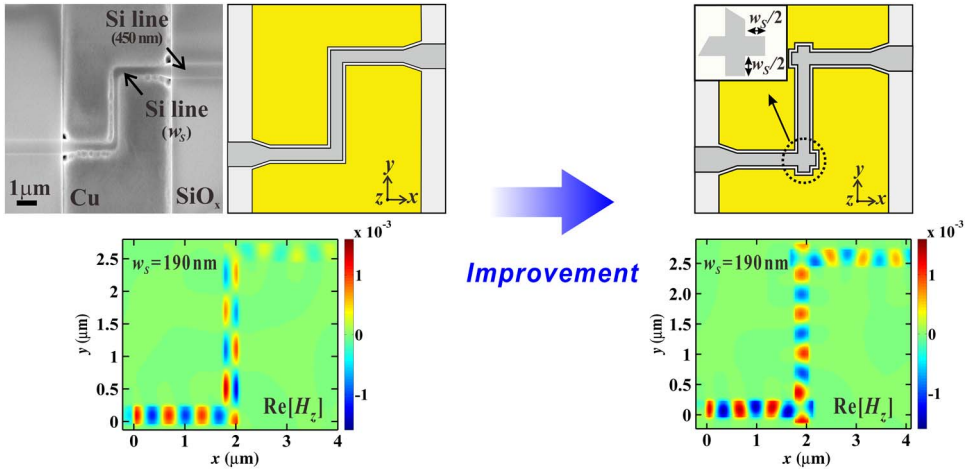


DOI: 10.1109/JPHOT.2013.2281983
1943-0655 

# Investigation and Improvement of 90° Direct Bends of Metal–Insulator–Silicon–Insulator–Metal Waveguides

**Jin-Soo Shin,[1] Min-Suk Kwon,[2] Chang-Hee Lee,[1] and Sang-Yung Shin[1]**

[1]Department of Electrical Engineering, Korea Advanced Institute of Science and Technology (KAIST), Daejeon 305-701, Korea
[2]School of Electrical and Computer Engineering, Ulsan National Institute of Science and Technology (UNIST), Ulsan 689-798, Korea

*DOI: 10.1109/JPHOT.2013.2281983*


Manuscript received August 12, 2013; revised September 6, 2013; accepted September 7, 2013. Date of publication September 16, 2013; date of current version October 1, 2013. This research was supported in part by Basic Science Program through the National Research Foundation of Korea (NRF) funded by the Ministry of Education, Science and Technology (NRF-2010-0022473) and in part by the 2012 Research Fund of the Ulsan National Institute of Science and Technology (UNIST). Corresponding author: M.-S. Kwon (e-mail: mskwon@unist.ac.kr).

**Abstract:** We investigate 90° direct bends of metal–insulator–silicon–insulator–metal (MISIM) waveguides, which are hybrid plasmonic waveguides with replaceable insulators. First, we fabricate them using fully standard CMOS technology and characterize them. The experimental excess loss of the two consecutive 90° direct bends is 11, 7.4, and 4.5 dB when the width of the Si line of the MISIM waveguide is about 160, 190, and 220 nm, respectively. Second, we analyze the experimental results using the 3-D finite-difference time-domain method. Through the analysis, we investigate possible loss mechanisms of the 90° direct bend, which have not been studied to our knowledge. It has been found that the Si lines should be narrow to reduce the excess losses of the 90° direct bends. However, the wide Si lines are better for ease of fabrication and for small propagation losses. Finally, we demonstrate a modified low-loss 90° direct bend of the MISIM waveguide with a wide Si line.

**Index Terms:** Plasmonics, silicon nanophotonics, subwavelength structure, waveguides.

## 1. Introduction

One possible way of overcoming the limit of electronic-only devices is to integrate electronic and photonic devices on a chip scale [1]. However, the dimensions of general photonic devices, which are subject to the diffraction limit, hinder such integration. Nanoplasmonic waveguides can support a mode with surface plasmon polariton nature whose dimensions are much smaller than those of a photonic waveguide mode [2]. Thus, it is expected that nanoplasmonic waveguide devices may alleviate the dimensional mismatch between photonic devices and electronic devices [3]. A variety of nanoplasmonic waveguides have been investigated. A few examples are channel plasmon polariton waveguides [4], dielectric-loaded surface plasmon polariton waveguides [5], [6], and metal–insulator–metal (MIM) waveguides [7]–[10]. However, a typical problem in these nanoplasmonic waveguides is that there is a tradeoff between the degree of mode confinement and the propagation distance. To some extent, the problem is solved by using hybrid plasmonic waveguides [11]–[19], which have a subwavelength mode size and a relatively long propagation distance compared with the aforementioned waveguides. Among diverse hybrid plasmonic waveguides, two

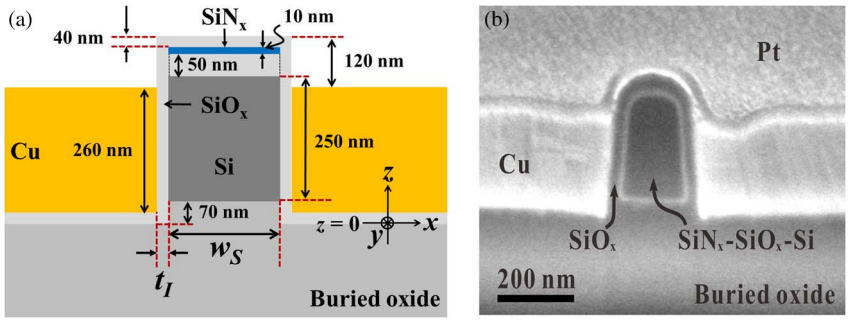


Fig. 1. (a) Schematic diagram of the cross-sectional structure of the realized MISIM waveguide. (b) SEM image of the cross section of the fabricated MISIM waveguide. Pt was just used for the preparation of the cross section, and it is not related to the MISIM waveguide.

kinds of metal–insulator–silicon–insulator–metal (MISIM) waveguides have been actively studied [16]–[19] since they can be realized by using standard CMOS technology. Zhu et al. have studied the covered MISIM waveguide, in which the metal surrounds the horizontal insulator–silicon–insulator stack [18], [19]. We have investigated the uncovered MISIM waveguide, in which the metal sandwiches laterally the horizontal insulator–silicon–insulator stack [16], [17]. Since the top surface of the insulator of this waveguide is exposed, the insulator is removable and replaceable with a functional material.

When nanoplasmonic devices that are based on the MISIM waveguides are developed, in general, they will have waveguide bends. In this paper, we investigate experimentally and theoretically 90° direct bends of the uncovered MISIM waveguides that have Si lines with widths of about 160, 190, and 220 nm. We show that such wide Si lines are not good for the simple 90° direct bends, although they make possible easy fabrication and small propagation losses of the MISIM waveguides. In doing so, we examine the loss mechanisms of the 90° direct bends, which have not yet been studied to our knowledge. In other words, we scrutinize how and why the excess losses of the 90° direct bends change depending on the width of the Si line and the distance between the two consecutive bends. Finally, we propose and analyze a modified 90° direct bend of the MISIM waveguide with a wide Si line to improve its performance.

## 2. Fabrication Process and Fabrication Results

The cross-sectional structure of the uncovered MISIM waveguide investigated in this paper is the same as in [17]. It is schematically shown in Fig. 1(a). A Si line of height 250 nm and of width $w_S$ is placed on a buried-oxide ridge of height about 70 nm. Because of the fabrication process used, ~10-nm-thick silicon nitride ($SiN_x$) and 50-nm-thick silicon oxide ($SiO_x$) layers are on the Si line. A $SiO_x$ layer that surrounds the $SiN_x-SiO_x-Si$ line becomes the insulator of the MISIM waveguide. The thickness of its horizontal parts is about 40 nm, and that of its vertical parts, i.e., $t_I$, is about 30 nm. On both sides of the $SiO_x-Si-SiO_x$ structure, there are copper layers of thickness about 260 nm. The MISIM waveguide supports a hybrid plasmonic mode. The power carried by the mode is strongly confined to the $SiO_x$ layers between the Si line and the Cu layers [16], [17]. To make the 90° direct bends of the MISIM waveguides, we used the same fabrication process as in [17], which is based on fully standard CMOS technology. They were made by using an 8-in silicon-on-insulator wafer. The fabrication process consists of low-pressure chemical vapor deposition (LPCVD), KrF (248 nm) lithography, dry etching, high-density plasma chemical vapor deposition (HDPCVD), sputtering, and chemical–mechanical polishing. Thin $SiN_x$ and $SiO_x$ layers were deposited by using LPCVD. We employed HDPCVD to deposit a thick $SiO_x$ layer that was patterned to be a mold for a copper damascene process. Copper was sputtered to fill the mold and polished chemically and mechanically until the top surface of the insulator was exposed. A scanning electron microscopy (SEM) image of the cross section of the fabricated MISIM waveguide is shown in Fig. 1(b), which is the same as in [17]. To make the overall process simple, we did not include a photoresist trimming

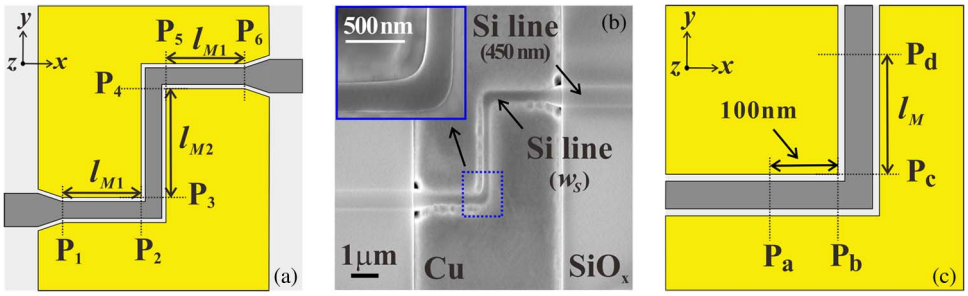


Fig. 2. (a) Schematic diagram of the structure of the MISIM waveguide with the two consecutive 90° direct bends on the *xy*-plane at $z = 195$ nm. (b) Surface SEM image of the fabricated MISIM waveguide with the 90° direct bends. The inset shows an enlarged image of the 90° direct bend. (c) Schematic diagram of the structure of the MISIM waveguide with one 90° direct bend on the *xy*-plane at $z = 195$ nm.

process after the KrF lithography. This results in larger values of $w_S$ than those in [18] and [19]. The resultant values of $w_S$ are about 160, 190, or 220 nm since 160 nm is the minimum line width that can be obtained from the KrF lithography.

Fig. 2(a) schematically shows the structure of the investigated MISIM waveguide with the two consecutive 90° direct bends on the *xy*-plane at $z = 195$ nm. Fig. 2(b) shows a surface SEM image of the fabricated MISIM waveguide with the 90° direct bends. The MISIM waveguide is connected to 450-nm-wide Si photonic waveguides through couplers in which $w_S$ increases linearly to 450 nm over a distance of 600 nm. The 450-nm-wide Si photonic waveguides are connected to 5-$\mu$m-wide Si photonic waveguides through linear tapering over a distance of 200 $\mu$m. Light from a source is launched into one 5-$\mu$m-wide Si photonic waveguide, and light from the other 5-$\mu$m-wide Si photonic waveguide is detected. The distance between the end of the coupler (position $P_1$) and the beginning of the 90° direct bend (position $P_2$) is $l_{M1}$. The distance between positions $P_5$ and $P_6$ is also $l_{M1}$. The distance between the end of one bend (position $P_3$) and the beginning of the other (position $P_4$) is $l_{M2}$. For the fabricated MISIM waveguide with the 90° direct bends, $l_{M1} = [(2\ \mu\text{m}) - w_S/2 - t_l]$ and $l_{M2} = [(2.5\ \mu\text{m}) - w_S - 2t_l]$. Consequently, the total length of the MISIM waveguide with the 90° direct bends, which is $2l_{M1} + 2(w_S + 2t_l) + l_{M2}$, is fixed at 6.5 $\mu$m.

## 3. Measurement and Simulation Results

We measured the fiber-to-fiber insertion losses (in dB) of the combinations of the 5-$\mu$m-wide Si photonic waveguides, the 450-nm-wide Si photonic waveguides, and the MISIM waveguide with or without the 90° direct bends. The length of the straight MISIM waveguide without the bends is 6.5 $\mu$m. An excess loss due to the two consecutive bends, denoted by $L_{b2}$, is defined as the subtraction of the insertion loss associated with the straight MISIM waveguide from that associated with the MISIM waveguide with the bends. To measure the fiber-to-fiber insertion losses, we launched light with a wavelength of 1554 nm from a lensed fiber to the facet of one 5-$\mu$m-wide Si photonic waveguide. Before the light was incident on the lensed fiber, its polarization was adjusted to be transverse electric using a polarization controller. The light coming out from the other 5-$\mu$m-wide Si photonic waveguide was coupled to another lensed fiber.

The experimental values of $L_{b2}$ are in Fig. 3 along with the calculated values. The error bars represent the standard deviation of the experimental values for the same value of $w_S$. For the calculation, we used the 3-D finite-difference time-domain (FDTD) method (FDTD Solutions, Lumerical Inc.). For the dielectric constant of copper, we used the model in FDTD Solutions, which is $-68.2 + i10.1$ at the wavelength of 1554 nm. While reducing mesh sizes, we checked the convergence of the calculation result. The smallest mesh sizes were 3, 3, and 5 nm along the *x*-, *y*-, and *z*-axes, respectively. We calculated the insertion losses (in dB) of the structure between $P_1$ and $P_6$ in Fig. 2(a). They were obtained from the ratios of the power of the light at $P_6$ to the power of the hybrid plasmonic mode, launched at $P_1$, of the MISIM waveguide. We also calculated the

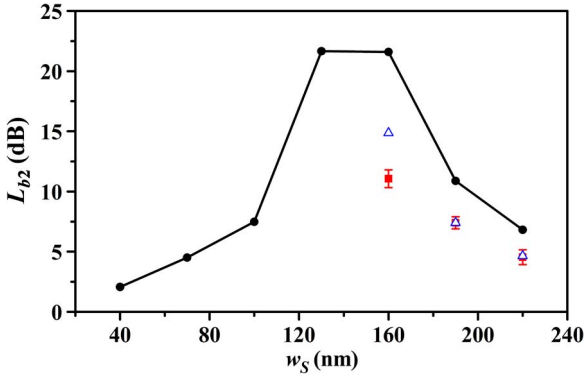


Fig. 3. Experimental and calculated values of $L_{b2}$ with respect to $w_S$. The experimental values are represented by the red square symbols with error bars. The theoretical values obtained from the 3-D FDTD simulation of the structure in Fig. 2(a) are also represented by the black solid lines with the circle symbols. The triangle symbols represent the calculated excess losses of the realized structure in Fig. 2(b) where the bends have the rounded corners.

propagation loss $\alpha_M$ (in dB/$\mu$m) of the straight MISIM waveguide. Following the definition of $L_{b2}$, we subtracted $[\alpha_M \times (6.5\ \mu\text{m})]$ from the insertion losses to obtain the calculated values of $L_{b2}$. The excess loss of one 90° direct bend may be approximately half of $L_{b2}$, i.e., 5.5, 3.7, and 2.25 dB for $w_S \cong 160$, 190, and 220 nm, respectively. As reported previously [17], the uncovered MISIM waveguide with the wide Si line has a smaller propagation loss than the covered MISIM waveguide with the narrow Si line. However, the 90° direct bend of the former causes a larger excess loss than the 90° direct bend of the latter, which causes an excess loss of $\sim 0.73 \pm 0.06$ dB when $t_l = 28$ nm and $w_S = 64$, 81, 94, or 102 nm [19]. Moreover, the experimental values of $L_{b2}$ are quite smaller than the calculated values. To explain these things and the increase and decrease of $L_{b2}$, we analyze how and why the excess loss of the 90° direct bend changes depending on its structural parameters. This kind of analysis for the MISIM waveguide bends has not yet been done.

First, we checked the reflection from one 90° direct bend and the transmission through it. For this purpose, we analyzed the MISIM waveguide with just one 90° direct bend, which is schematically shown in Fig. 2(c). Positions $P_b$ and $P_c$ in Fig. 2(c) correspond to $P_2$ and $P_3$ in Fig. 2(a), respectively. We launched the hybrid plasmonic mode at position $P_a$, which is 100 nm to the left of $P_b$, and we calculated the power of the left-going light at $P_a$. Reflectivity is defined as the ratio of this power to the launched power. Position $P_d$ is located at a distance $l_M$ above $P_c$. When $l_M = 100$ nm, we calculated the power of the light at $P_d$. Transmittance is defined as the ratio of this power to the launched power. Fig. 4(a) shows the reflectivity and the transmittance with respect to $w_S$. The reflectivity increases as the transmittance decreases, and vice versa. Their sum remains almost constant and is smaller than 1 because of a loss in the region between $P_a$ and $P_d$. The increase in reflectivity with $w_S$ is similar to what is observed in a 90° direct bend of a MIM waveguide [7]. As the insulator width of the MIM waveguide increases, the transmission through the 90° direct bend decreases while the reflection from the bend increases. (It was also confirmed in our numerical simulation of the 90° direct bend of the MIM waveguide.)

Next, we calculated the excess loss $L_{b1}$ of the MISIM waveguide with one 90° direct bend as a function of $l_M$. The excess loss $L_{b1}$ is defined as the subtraction of $[\alpha_M \times (100\ \text{nm} + w_S + 2t_l + l_M)]$ from the insertion loss (in dB) of the structure between $P_a$ and $P_d$. Fig. 4(b) and (c) shows the calculated curves of $L_{b1}$ for a few values of $w_S$ within the range [40 nm, 220 nm]. As $w_S$ increases up to 130 nm, $L_{b1}$ at $l_M = 100$ nm increases due to the increase in reflectivity. For $w_S \leq 130$ nm, $L_{b1}$ slightly increases initially with $l_M$ and soon becomes almost constant. However, as $w_S$ increases further, $L_{b1}$ at $l_M = 100$ nm decreases due to the decrease in reflectivity. For $w_S > 130$ nm, $L_{b1}$ keeps increasing with $l_M$. This is different from what is expected from ordinary excess losses.

To find a reason for the increase of $L_{b1}$ with $l_M$, we calculated the electric field distribution of the transmitted light along the MISIM waveguide with the hybrid plasmonic mode launched at $P_a$. For

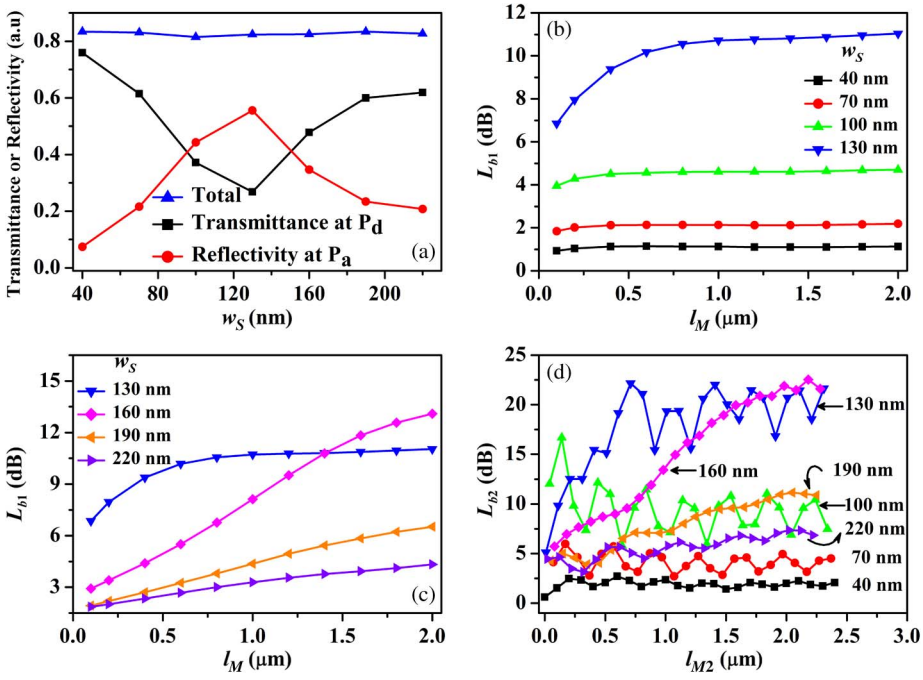


Fig. 4. (a) Reflectivity and transmittance of one 90° direct bend versus $w_S$. The sum of the reflectivity and the transmittance is also drawn together. (b) and (c) Calculated relations of $L_{b1}$ to $l_M$ for several values of $w_S$ in the case of the MISIM waveguide with one 90° direct bend. (d) Calculated relations of $L_{b2}$ to $l_{M2}$ for several values of $w_S$ in the case of the MISIM waveguide with the two consecutive 90° direct bends. The meanings of the symbols in (d) are the same as in (b) and (c).

different values of $w_S$, Fig. 5(a) shows the distributions of Re$[E_x]$ after $P_c$, where $E_x$ represents the $x$-component of the electric field, on the $xy$-plane at $z = 195$ nm. The insets in Fig. 5(a) show the distributions of Re$[E_x]$ on the $xz$-plane at the positions denoted by the dashed lines. As $w_S$ increases, the distributions become more and more asymmetric about the $z$-axis. For example, the distribution is almost symmetric for $w_S = 40$ nm; however, it is almost antisymmetric for $w_S = 220$ nm. After the bend, not only the hybrid plasmonic mode but also antisymmetric radiation modes are excited. For more information, modes that exist in a bounded region containing the MISIM waveguide were analyzed by using the mode solver of FDTD Solutions, which is based on the finite-difference method. For $w_S < 230$ nm, the hybrid plasmonic mode is the only guided mode of the MISIM waveguide. Other modes have effective indexes with real parts smaller than the refractive index of the buried oxide or substrate. Thus, they are radiation modes whose fields radiate into the substrate. The distributions of Re$[E_x]$ of antisymmetric radiation modes are shown in Fig. 5(b), and their effective indexes $(N_a)$ are summarized in Table 1 along with those $(N_h)$ of the hybrid plasmonic mode. As $w_S$ decreases, the imaginary part of $N_a$ increases so that the decay of the antisymmetric radiation mode becomes fast.

As deduced in Figs. 4 and 5, for $w_S < 130$ nm, the hybrid plasmonic mode incident on the bend is mainly transferred and reflected to the same mode. Although antisymmetric radiation modes are excited because of the bend, they decay out rapidly. However, for $w_S > 130$ nm, antisymmetric radiation modes are dominantly excited after the bend. In this case, the bend behaves similarly as a mode converter. Hence, the excess loss $L_{b1}$ for $w_S > 130$ nm means how efficiently the hybrid plasmonic mode is converted to antisymmetric radiation modes and how fast they decay compared with the hybrid plasmonic mode. Since the imaginary part of $N_a$ is larger than that of $N_h$, $L_{b1}$ increases with $l_M$. The dominant excitation of antisymmetric radiation modes for $w_S > 130$ nm might be explained intuitively as follows. A large portion of the power carried by the MISIM waveguide mode is transported along the insulator. Between $P_b$ and $P_c$, the part of the light along the outer insulator travels a longer distance than the part of the light along the inner insulator. The optical path

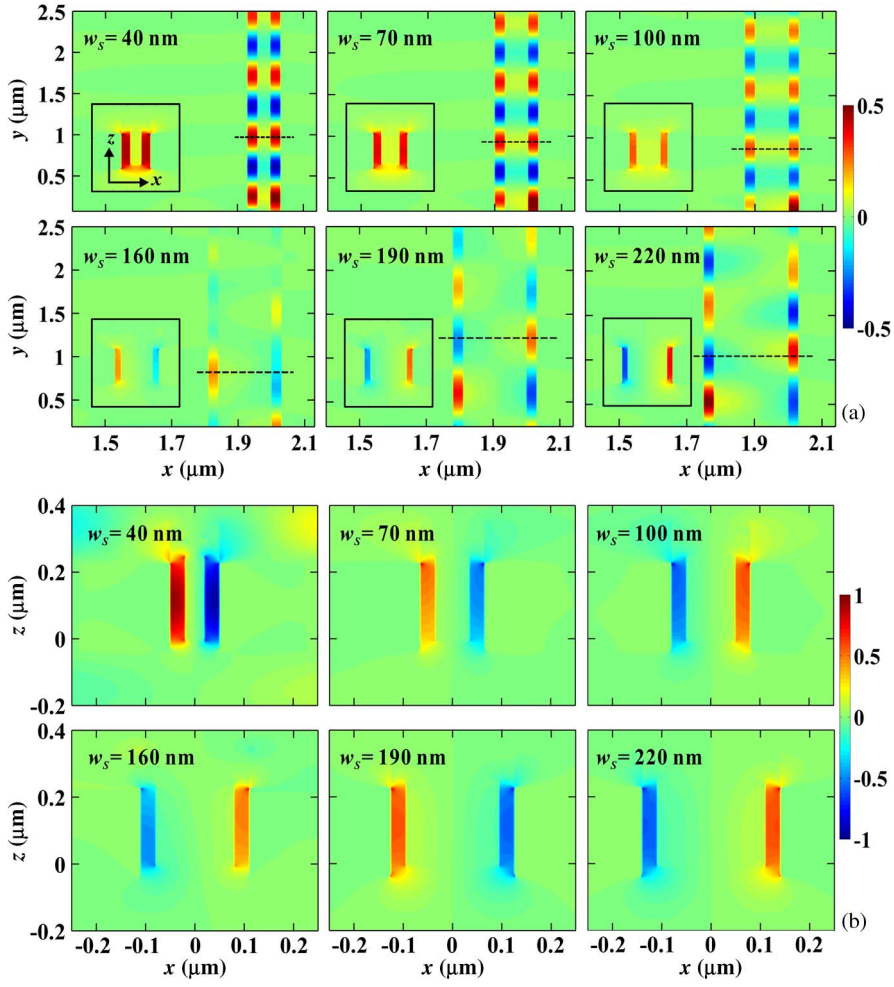


Fig. 5. (a) Distributions of Re$[E_x]$ on the $xy$-plane at $z = 195$ nm after the 90° direct bends for $w_S = 40$, 70, 100, 160, 190, and 220 nm. The insets show the distributions of Re$[E_x]$ on the $xz$-plane at the positions denoted by the dashed lines. (b) Distributions of Re$[E_x]$ of antisymmetric radiation modes for the same values of $w_S$ as those in (a).

TABLE 1

Effective indexes of the hybrid plasmonic mode $(N_h)$ and antisymmetric radiation modes $(N_a)$

| $w_S$ | Re$[N_h]$ | Im$[N_h]$ | Re$[N_a]$ | Im$[N_a]$ |
|---|---|---|---|---|
| 40 nm | 2.070 | 0.039 | 0.007 | 3.770 |
| 70 nm | 2.131 | 0.035 | 0.025 | 2.219 |
| 100 nm | 2.193 | 0.032 | 0.044 | 1.471 |
| 160 nm | 2.300 | 0.026 | 0.656 | 0.075 |
| 190 nm | 2.346 | 0.023 | 1.167 | 0.057 |
| 220 nm | 2.394 | 0.020 | 1.401 | 0.046 |

difference between the two parts is about 2Re$[N_h](w_S + t_l)$. For $w_S$ about 160 nm, it is close to half the wavelength so that the two parts have a phase difference of $\pi$ at $P_c$. In this way, the hybrid plasmonic mode at $P_b$ is converted to antisymmetric radiation modes. Based on this intuitive explanation, in the next section, we modify the 90° direct bend with a large value of $w_S$ to reduce its excess loss.

Because of the reflection from the 90° direct bend and the excitation of antisymmetric radiation modes after the 90° direct bend, the excess loss $L_{b2}$ changes depending on $l_{M2}$. To check this, we calculated $L_{b2}$ as a function of $l_{M2}$. The calculated relations of $L_{b2}$ to $l_{M2}$ for different values of $w_S$ are in Fig. 4(d). For $w_S < 130$ nm, the additional reflection from the second bend makes $L_{b2}$ almost twice as large as $L_{b1}$ in Fig. 4(b). The multiple reflections between the two bends cause the MISIM waveguide with the two bends to behave similarly as a Fabry–Perot resonator. Consequently, $L_{b2}$ fluctuates as $l_{M2}$ increases. This fluctuation becomes large as $w_S$ increases up to 130 nm since the reflectivity of the bend increases with $w_S$, as shown in Fig. 4(a). For $w_S > 130$ nm, we checked that the antisymmetric radiation modes excited by the first bend are reciprocally converted to the hybrid plasmonic mode after the second bend. In this case, $L_{b2}$ is also larger than $L_{b1}$ and fluctuates slightly due to the second bend. In addition, $L_{b2}$ increases with $l_{M2}$ since antisymmetric radiation modes with propagation losses larger than that of the hybrid plasmonic mode travel between the two bends.

As shown in the inset in Fig. 2(b), the outer and inner corners of the realized 90° direct bend are not sharp, but they are rounded. Such rounded corners make the experimental values of $L_{b2}$ smaller than the calculated values. We modified the simulated structure of the 90° direct bend to make it close to the realized one, and then, we calculated $L_{b2}$. The calculated values of $L_{b2}$ are 14.8, 7.4, and 4.6 dB for $w_S = 160$, 190, and 220 nm, respectively. They are represented in Fig. 3 and in good agreement with the experimental values.

Through the various calculations, we have shown that the reflection from the 90° direct bend is a main loss mechanism of the 90° direct bend for $w_S < 130$ nm. This explains the increase of $L_{b2}$ in Fig. 3. When the two bends are connected, the excess loss due to them $(L_{b2})$ changes significantly with the distance between them $(l_{M2})$ because of the multiple reflections. For $w_S > 130$ nm, the 90° direct bend causes the conversion between the hybrid plasmonic mode and antisymmetric radiation modes. $L_{b2}$ increases with $l_{M2}$ because of the large propagation losses of antisymmetric radiation modes. Hence, the mode conversion is a main loss mechanism of the 90° direct bends for $w_S > 130$ nm. This explains the decrease of $L_{b2}$ in Fig. 3.

## 4. Modified 90° Direct Bend

The simulation results show that the MISIM waveguide with the narrow Si line is better for the 90° direct bend than that with the wide Si line from the viewpoint of excess losses. For example, as shown in Fig. 3, $L_{b2} = 2.1$ dB for $w_S = 40$ nm, but $L_{b2} = 10.8$ dB for $w_S = 190$ nm. Although the 90° direct bend with $w_S = 40$ nm causes a small excess loss, its total insertion loss, which is the sum of the excess loss and the total propagation loss, is large. This is because the propagation loss of the MISIM waveguide increases as $w_S$ decreases. In addition, the MISIM waveguide devices with narrow Si lines require an additional fabrication process such as photoresist trimming, compared with those with wide Si lines. Therefore, for small total insertion losses and ease of fabrication, the 90° direct bend of the MISIM waveguide with the wide Si line must be modified to suppress the mode conversion.

Using the aforementioned explanation of the excitation of antisymmetric radiation modes, we modified the bend as shown in Fig. 6(a). The modified bend has two protrusions of length $w_S/2$ on its outer corner. Except for these protrusions, the structure in Fig. 6(a) is the same as the structure in Fig. 2(a), which was used to get the result in Fig. 3. The protrusions may be considered to make the optical path length along the outer insulator about one wavelength longer than that along the inner insulator. Consequently, the two parts of the light traveling along the inner and outer insulators are in phase. Hence, the excitation of antisymmetric radiation modes seems to be suppressed. This can be checked in Fig. 6(b) and (c). The distribution of $\mathrm{Re}[E_x]$ after the modified bend is almost symmetric in contrast to that after the simple bend in Fig. 5(a). The distribution of $\mathrm{Re}[H_z]$, where $H_z$ is the real part of the $z$-component of the magnetic field, also indicates that the hybrid plasmonic mode is well excited after the modified bends. In this way, the excess loss of the modified bends can be reduced. When $w_S = 190$ nm, the structure in Fig. 6(a) has the calculated excess loss of 2.7 dB. When $w_S = 40$ nm, the structure in Fig. 2(a) has the calculated excess loss of 2.1 dB.

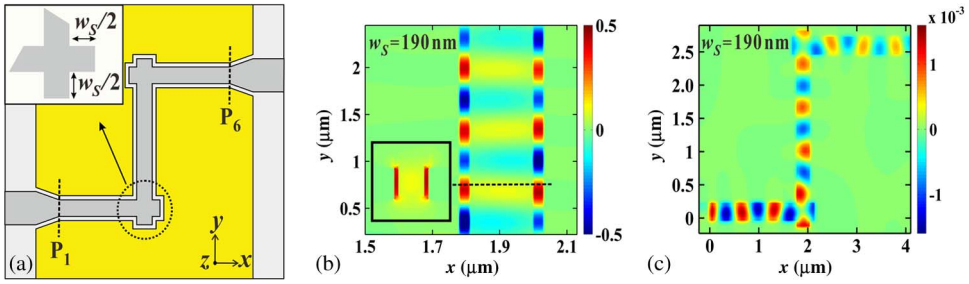


Fig. 6. (a) Schematic diagram of the structure of the MISIM waveguide with the modified bends on the *xy*-plane at $z = 195$ nm. (b) Distribution of Re$[E_x]$ on the *xy*-plane at $z = 195$ nm after the modified 90° direct bend with $w_S = 190$ nm. The inset shows the distribution of Re$[E_x]$ on the *xz*-plane at the position denoted by the dashed line. (c) Distribution of Re$[H_z]$ on the *xy*-plane at $z = 195$ nm.

However, the total insertion loss of the structure in Fig. 6(a) is 3.1 dB smaller than that of the structure in Fig. 2(a). These results indicate that the modification improves the performance of the 90° direct bend of the MISIM waveguide with the wide Si line. They also indicate that the explanation based on the excitation of antisymmetric radiation modes is reasonable. Finally, it is meaningful to compare the modified bend and a Si photonic waveguide bend. The single modified bend has an excess loss of about 1.3 dB while it occupies an area of $(3w_S/2 + 2t_l)^2 = 0.12\ \mu\text{m}^2$. However, the 90° curved bend of a Si photonic waveguide has an excess loss of about 0.1 dB if its bending radius is 1 $\mu$m while it occupies an area of 1.56 $\mu\text{m}^2$ [20]. Therefore, the modified bend is more advantageous in respect of compactness than the curved bend although the former has a larger excess loss than the latter.

## 5. Conclusion

We fabricated the 90° direct bends of the uncovered MISIM waveguides, using fully standard CMOS technology without an additional photoresist trimming process. We measured the excess loss of the two consecutive 90° direct bends, which is 11, 7.4, and 4.5 dB for $w_S \cong 160$, 190, and 220 nm, respectively. Through the various calculations based on the 3-D FDTD method, newly we have investigated the loss mechanisms of the 90° direct bends. If the Si line of the MISIM waveguide is narrower than 130 nm, the excess loss of the 90° direct bend is caused by the reflection from the bend. If the Si line is wider than 130 nm, the excess loss of the two consecutive bends is caused by the excitation of antisymmetric radiation modes between the bends. Our investigation has indicated that a narrow Si line (e.g., with a width of 40 nm) is desirable for reducing the excess loss of the 90° direct bend. However, a wide Si line (e.g., with a width of 190 nm) is better for ease of fabrication and small propagation losses. Hence, for the MISIM waveguide with the wide Si line, we have proposed the modified 90° direct bend. Based on the numerical simulation, we have confirmed that it has small excess loss similar to that of the simple 90° direct bend of the MISIM waveguide with the narrow Si line. It is promising in that it is easy to fabricate and has a small total insertion loss, in comparison with the 90° direct bend of the MISIM waveguide with the narrow Si line.

## References

[1] M. L. Brongersma and V. M. Shalaev, "The case for plasmonics," *Science*, vol. 328, no. 5977, pp. 440–441, Apr. 2010.
[2] E. Ozbay, "Plasmonics: Merging photonics and electronics at nanoscale dimensions," *Science*, vol. 311, no. 5758, pp. 189–193, Jan. 2006.
[3] M. Dragoman and D. Dragoman, "Plasmonics: Applications to nanoscale terahertz and optical devices," *Prog. Quantum Electron.*, vol. 32, no. 1, pp. 1–41, Jan. 2008.
[4] S. I. Bozhevolnyi, V. S. Volkov, E. Devaux, J.-Y. Laluet, and T. W. Ebbesen, "Channel plasmon subwavelength waveguide components including interferometers and ring resonators," *Nature*, vol. 440, no. 7083, pp. 508–511, Mar. 2006.
[5] T. Holmgaard and S. I. Bozhevolnyi, "Theoretical analysis of dielectric-loaded surface plasmon-polariton waveguides," *Phys. Rev. B*, vol. 75, no. 24, pp. 245405-1–245405-12, Jun. 2007.

[6] R. M. Briggs, J. Grandidier, S. P. Burgos, E. Feigenbaum, and H. A. Atwater, "Efficient coupling between dielectric-loaded plasmonic and silicon photonic waveguides," *Nano Lett.*, vol. 10, no. 12, pp. 4851–4857, Oct. 2010.
[7] G. Veronis and S. Fan, "Bends and splitters in metal–dielectric–metal subwavelength plasmonic waveguides," *Appl. Phys. Lett.*, vol. 87, no. 13, pp. 131102-1–131102-3, Sep. 2005.
[8] S. I. Bozhevolnyi and J. Jung, "Scaling for gap plasmon based waveguides," *Opt. Exp.*, vol. 16, no. 4, pp. 2676–2684, Feb. 2008.
[9] Z. Han, A. Y. Elezzabi, and V. Van, "Experimental realization of subwavelength plasmonic slot waveguides on a silicon platform," *Opt. Lett.*, vol. 35, no. 4, pp. 502–504, Feb. 2010.
[10] D. R. Mason, D. K. Gramotnev, and K. S. Kim, "Wavelength-dependent transmission through sharp 90° bends in sub-wavelength metallic slot waveguides," *Opt. Exp.*, vol. 18, no. 15, pp. 16 139–16 145, Jul. 2010.
[11] R. F. Oulton, V. J. Sorger, D. A. Genov, D. F. P. Pile, and X. Zhang, "A hybrid plasmonic waveguide for subwavelength confinement and long-range propagation," *Nat. Photon.*, vol. 2, no. 8, pp. 496–500, Jul. 2008.
[12] D. Dai and S. He, "A silicon-based hybrid plasmonic waveguide with a metal cap for a nano-scale light confinement," *Opt. Exp.*, vol. 17, no. 19, pp. 16 646–16 653, Sep. 2009.
[13] M. Wu, Z. Han, and V. Van, "Conductor-gap-silicon plasmonic waveguides and passive components at subwavelength scale," *Opt. Exp.*, vol. 18, no. 11, pp. 11 728–11 736, May 2010.
[14] D. Dai and S. He, "Low-loss hybrid plasmonic waveguide with double low-index nano-slots," *Opt. Exp.*, vol. 18, no. 17, pp. 17 958–17 966, Aug. 2010.
[15] X.-Y. Zhang, A. Hu, J. Z. Wen, T. Zhang, X.-J. Xue, Y. Zhou, and W. W. Duley, "Numerical analysis of deep sub-wavelength integrated plasmonic devices based on semiconductor–insulator–metal strip waveguides," *Opt. Exp.*, vol. 18, no. 18, pp. 18 945–18 959, Aug. 2010.
[16] M.-S. Kwon, "Metal–insulator–silicon–insulator–metal waveguides compatible with standard CMOS technology," *Opt. Exp.*, vol. 19, no. 9, pp. 8379–8393, Apr. 2011.
[17] M.-S. Kwon, J.-S. Shin, S.-Y. Shin, and W.-G. Lee, "Characterizations of realized metal–insulator–silicon–insulator–metal waveguides and nanochannel fabrication via insulator removal," *Opt. Exp.*, vol. 20, no. 20, pp. 21 875–21 887, Sep. 2012.
[18] S. Zhu, T. Y. Liow, G. Q. Lo, and D. L. Kwong, "Silicon-based horizontal nanoplasmonic slot waveguides for on-chip integration," *Opt. Exp.*, vol. 19, no. 9, pp. 8888–8902, Apr. 2011.
[19] S. Zhu, G. Q. Lo, and D. L. Kwong, "Components for silicon plasmonic nanocircuits based on horizontal Cu-SiO2-Si-SiO2-Cu nanoplasmonic waveguides," *Opt. Exp.*, vol. 20, no. 6, pp. 5867–5881, Mar. 2012.
[20] Z. Sheng, D. Dai, and S. He, "Comparative study of losses in ultrasharp silicon-on-insulator nanowire bends," *IEEE J. Sel. Topics Quantum Electron.*, vol. 15, no. 5, pp. 1406–1412, Sep./Oct. 2009.